AWARD NUMBER: W81XWH-15-1-0009

TITLE: Photovoltaic Retinal Prosthesis for Restoring Sight to Patients Blinded by Retinal Injury or Degeneration

PRINCIPAL INVESTIGATOR: Prof. Daniel Palanker

CONTRACTING ORGANIZATION: Leland Stanford Junior University
Stanford, CA 94305

REPORT DATE: February 2017

TYPE OF REPORT: Annual

PREPARED FOR: U.S. Army Medical Research and Materiel Command
Fort Detrick, Maryland 21702-5012

REPORT DOCUMENTATION PAGE

Form Approved
OMB No. 0704-0188

1. REPORT DATE	2. REPORT TYPE	3. DATES COVERED
Feb 2017	Annual	1 Feb 2016 - 31 Jan 2017

4. TITLE AND SUBTITLE

Photovoltaic Retinal Prosthesis for Restoring Sight to Patients Blinded by Retinal Injury or Degeneration

5a. CONTRACT NUMBER

5b. GRANT NUMBER
W81XWH-15-1-0009

5c. PROGRAM ELEMENT NUMBER

6. AUTHOR(S)

Prof. Daniel V. Palanker

E-Mail:palanker@stanford.edu

5d. PROJECT NUMBER

5e. TASK NUMBER

5f. WORK UNIT NUMBER

7. PERFORMING ORGANIZATION NAME(S) AND ADDRESS(ES)

Stanford University,
Astro-Physics Building, 452 Lomita Mall,
Stanford, CA 94305-4085

8. PERFORMING ORGANIZATION REPORT NUMBER

9. SPONSORING / MONITORING AGENCY NAME(S) AND ADDRESS(ES)

U.S. Army Medical Research and Materiel Command
Fort Detrick, Maryland 21702-5012

10. SPONSOR/MONITOR'S ACRONYM(S)

11. SPONSOR/MONITOR'S REPORT NUMBER(S)

12. DISTRIBUTION / AVAILABILITY STATEMENT

Approved for Public Release; Distribution Unlimited

13. SUPPLEMENTARY NOTES

14. ABSTRACT:

Ocular trauma can result in traumatic retinopathy, which, like retinal degeneration, leads to blindness due to loss of photoreceptors. Visual information can be reintroduced into the retina by patterned electrical stimulation of the remaining inner retinal neurons. Photovoltaic subretinal prosthesis directly converts light into pulsed electric current in each pixel, stimulating the nearby neurons. Images captured by the head-mounted camera are projected onto retina by video goggles using pulsed near-infrared (~880nm) light. Preparation of this technology for clinical trial requires optimization of the photovoltaic array, addition of the biocompatible protective coating for long-term implantation in human patients, fabrication of the video goggles with a camera, and image processing software. In particular, we are working on (1) Development and testing of the SiC protective biocompatible coating for the implant. (2) Optimization of the pixel configuration to maximize its performance, including the light-to-current conversion, dynamic range, maximum repetition rate, minimum cross-talk and minimum pixel size. (3) Development of the near-infrared pulsed video goggles. (4) Development of the image processing software and user interface.

15. SUBJECT TERMS

16. SECURITY CLASSIFICATION OF:			17. LIMITATION OF ABSTRACT	18. NUMBER OF PAGES	19a. NAME OF RESPONSIBLE PERSON
a. REPORT	b. ABSTRACT	c. THIS PAGE			USAMRMC
Unclassified	Unclassified	Unclassified	Unclassified	15	19b. TELEPHONE NUMBER *(include area code)*

Table of Contents

Page

Introduction

Ocular trauma can result in traumatic retinopathy, which, like retinal degeneration, leads to blindness due to loss of photoreceptors. Visual information can be reintroduced into the retina by patterned electrical stimulation of the remaining inner retinal neurons. Photovoltaic subretinal prosthesis directly converts light into pulsed electric current in each pixel, stimulating the nearby neurons. Images captured by the head-mounted camera are projected onto retina by video goggles using pulsed near-infrared (~880nm) light. Preparation of this technology for clinical trial requires optimization of the photovoltaic array, addition of the biocompatible protective coating for long-term implantation in human patients, fabrication of the video goggles with a camera, and image processing software. In particular, we are working on (1) Development and testing of the SiC protective biocompatible coating for the implant. (2) Optimization of the pixel configuration to maximize its performance, including the light-to-current conversion, dynamic range, maximum repetition rate, minimum cross-talk and minimum pixel size. (3) Development of the near-infrared pulsed video goggles. (4) Development of the image processing software and user interface.

Keywords

Retinal prosthesis, photovoltaic, retinal degeneration, traumatic retinopathy, restoration of sight.

Major goals of the project

Major Task 1: Development and testing of the SiC protective biocompatible coating for the implant

Subtask 1

a) Coat the implant with amorphous SiC to prevent erosion.
b) Test erosion of the coated and uncoated implants using accelerated aging at elevated temperature for 12 days, equivalent to 12 months at physiological conditions.
c) Test erosion of the coated and uncoated implants in-vivo during 6-12 months.

Subtask 2

a) Test biocompatibility of the SiC coating using subretinal implantation in the wild type (Long Evans) and RCS rats for 3-12 months. Retinal thickness and potential appearance of the subretinal gliosis or fibrosis will be monitored in-vivo using OCT. Health of the retinal vasculature and potential damage to RPE at the edges of the implant will be monitored using fluorescein angiography and autofluorescence.
b) After enucleation, study retinal structure above the implant using confocal microscopy with immunohistochemical staining of the sample.
c) In the case of poor biocompatibility we will add an additional layer of parylene on top of SiC, leaving only the electrodes exposed.

Major Task 2: Optimization of the pixel configuration to maximize its performance, such as light-to-current conversion efficiency, dynamic range, maximum repetition rate, and minimum cross-talk.

Subtask 1

a) Using computational model of the equivalent optoelectronic circuit, optimize the number of diodes, sizes of the active and return electrodes and the exposed silicon area to maximize the output current, charge injection, and dynamic range of modulation.

b) Using computational model of the equivalent optoelectronic circuit, optimize the value of the shunt resistor for sufficiently fast discharge between the pulses, while on the other hand, not draining too much current away from the tissue during the light pulse itself. The target frequency in this optimization corresponds to the perceptual flicker fusion observed in the range of 20-40 Hz.

Subtask 2

Using computational model of electric field in tissue, optimize connectivity of the return electrodes and the size of the metalized areas on the side and back walls of the implant to minimize the cross-talk of the neighboring pixels and to maximize the field penetration into the retina.

Subtask 3

a) Manufacture optimized photovoltaic arrays
b) Verify optoelectronic performance of the photovoltaic arrays experimentally in a saline solution.
c) Verify optoelectronic performance of the photovoltaic arrays in-vivo by measuring electrical waveforms produced by the implant using corneal electrodes. The same animals with the subretinal implants will be used here, as the ones described in the Task 1/2/a

Major Task 3: Development of the NIR video goggles

Subtask 1

a) Develop video goggles with bright pulsed NIR (880-905nm) illumination.
b) Ensure ocular safety in the event of a critical failure of the display.
c) Assess the visual field, brightness and contrast of the projected images on the retina.

Major Task 4: Development of the image processing software and user interface

Subtask 1

a) Using information from our electrophysiological studies regarding spatial and temporal summation of the spot stimuli in a pattern, optimize the spatial and temporal sequence of the pixel activation to provide the highest dynamic range and contrast.
b) Develop image processing to maximize the user's ability to accomplish daily tasks such as reading, face recognition, navigating an unfamiliar environment. Software should extract or enhance critical aspects of the image to be displayed in a crisper form to the user, such as text, simplified images of the objects matching the resolution limitations of the implant.

Subtask 2

a) Develop the graphic user interface for the technician and for the patient. The GUI will allow adjustment of the image processing software, including the following parameters: (a) resolution, (b) dynamic range of brightness and the number of gray levels, (c) spatial filtering (edge enhancement, image sparsity, thresholding), (d) frame rate, sub-division of the frames, and pulse frequency.
b) Evaluate a possibility of including the voice control and/or gesture recognition into the user interface.
c) Test the image processing software and the user interfaces on healthy volunteers (3-4 members of the research team) using conventional video goggles with a similar visual field.

Accomplishments

1. **Verification of the photovoltaic implant performance by measurement of the contrast sensitivity of prosthetic vision ex-vivo**

Introduction

We developed a completely wireless approach based on subretinally placed photodiode arrays, which photovoltaicly convert projected image into electric current flowing through the retina between the active and return electrode in each pixel to stimulate the nearby inner retinal neurons[7,8]. Images captured by the camera are processed and projected onto the retina from video goggles using near-infrared (NIR, 880-915nm) light to avoid photophobic and phototoxic effects of by bright illumination[9].

Previously we demonstrated retinal adaptation to high frequency (>20Hz) subretinal stimulation[10,11] as opposed to direct stimulation of ganglion cells, which can follow stimulation at rates exceeding 100Hz[12]. Adaptation to subretinal stimulation is similar to flicker fusion occurring with normal vision at high frequencies, which allows continuous perception of movies composed of static frames. This feature is critical for prosthetic vision since electrical stimulation has to be pulsed in order to preserve charge balanced and thereby avoid irreversible electrochemical reactions at the electrode-electrolyte interface.

One of the important characteristics of vision in general, and of prosthetic vision in particular, is contrast sensitivity. With a carrier frequency above flicker fusion, contrast can be modulated by slow adjustments of either the amplitude or duration of the pulsed stimuli. In a previous *ex-vivo* study we measured the increase in spiking rate with increasing irradiance, and the corresponding contrast was about 60%, as opposed to 3% with natural vision in rodents[13]. However, these measurements did not quantify other changes in the RGCs firing patterns. Here we revisit the measurements of contrast sensitivity using a novel analysis of the firing patterns in prosthetic and natural vision, and demonstrate significantly higher contrast sensitivity.

Methods

Photovoltaic implants

The 1 and 2mm-wide arrays of 30μm in thickness with photovoltaic pixels of 70, 140 and 280μm in size were manufactured according to the previously described methods[14], except for reversal of the n- and p-doped regions to produce anodic-first pulses. In these measurements, we used arrays of 1 mm in diameter with 70μm pixels.

Electrophysiological Recordings

A small piece of RCS or WT rat retina (~3mm x 3mm) was isolated and placed on a 512-electrode recording array (MEA)[15] ganglion cell side down. The retina was constantly perfused with Ames' medium at 29.4 °C and bubbled with a mixture of 95% O2 and 5% C02. For assessment of prosthetic vision, a photovoltaic implant was placed on top of the retina, mimicking a subretinal placement *in-vivo*[7]. We used a nylon mesh (~100um cell size) to lightly press the implant and retina onto the MEA to achieve good contact. The same procedures were undertaken for natural vision without the implant in place. Voltage waveforms were amplified and digitized with 20 kHz sampling frequency for each of the 512 electrodes on the MEA.[15]

For prosthetic vision, the 880 nm diode laser coupled via a 400-μm multimode fiber was used for illumination. The beam exiting from the fiber was collimated, homogenized using a 2° divergence microlens array diffuser, and projected onto the implant via the camera port of an inverted microscope. The projection system was calibrated to deliver upto a maximum power of 8mW/mm^2 onto the sample. For single-pulse stimulation, 4-ms square NIR pulses were applied at 1 Hz repetition rate, and *n=120* trials were used to determine the RGC responses. For contrast

sensitivity measurements, we used a carrier waveform consisting of 4-ms square NIR pulses applied at 20 Hz. Contrast steps were constructed by modulating the amplitude (peak power) with 0.5-second-long phase of 8mW/mm^2, followed by a 0.5-second-long phase of a chosen lower light intensity, and then return to 8mW/mm^2. We used *n=80* trials for every contrast step.

For natural vision, the image of a 15" CRT screen was optically reduced in size and projected onto the photoreceptor layer of a healthy retina through the camera port of the inverted microscope. Modulation of light intensity was performed with 0.5-second-long steps, similar to the envelop of prosthetic stimulation. In addition to full-field light intensity steps, we stimulated WT retinas with spatiotemporal monochromatic white noise using 70x70μm pixels refreshed every 33ms in order to differentiate between ON- and OFF-center RGC types[17].

Data Analysis

Raw recording traces from prosthetic stimulation were first subjected to electrical stimulation artifact removal. For every individual electrical pulse and electrode, we estimated the artifact by fitting a 7th-order polynomial to the data between 8.25 ms and 50 ms proceeding the onset of the pulse. The fitted polynomial was then subtracted from the raw voltage trace. Since an overly large artifact during the first 8.25 ms following the onset of pulse could not be removed, we replaced that portion with a randomly generated noise. As a result, action potentials (spikes) elicited during that period were discarded.

The artifact-subtracted traces were then used for spike detection and sorting using custom software described previously[15]. Spikes were defined as an event where the negative voltage deflection amplitude exceeded 3 times root-mean-squared noise on each electrode. We applied dimensionality reduction to the detected spike waveforms using principal component analysis, followed by expectation-maximization clustering[15,18]. For each putative neuron, we calculated the electrophysiological image (EI) of the neuron - the average electrical signal measured on the whole multielectrode array when the neuron produced an action potential. It typically shows the soma location and axonal trajectory of the RGC[19-21]. Neurons with abnormal EIs were excluded from our analysis. Responses of neurons to prosthetic stimulation were manually classified according to their raster response properties. For visible light stimulation, cells were classified as ON- and OFF-center types based on polarity of the first peak in the spike-triggered average (STAs) traces.

We used the Michelson definition for contrast $(I_{post} - I_{pre})/(I_{post} + I_{pre})$, where I_{pre} and I_{post} are the luminances (or peak irradiance for prosthetic stimulation) preceding or following the contrast step, respectively. To assess cellular response to prosthetic stimulation, we compared the distributions of spike rates 250 ms before and after a contrast step. The spike times were binned over 80 trials, and the resulting histograms were compared using the two-sample Kolmogorov-Smirnov test. Bin widths varying between 5 and 12.5 ms were compared and optimized to yield minimal *p*-values. For visible light stimulation, the activity of a cell subjected to 0.5% contrast was considered as the baseline spontaneous firing rate. Firing pattern of each RGC from 25 ms to 250 ms post-contrast step was compared to its baseline, using the same statistical method as for electrical stimulation. The first 25 ms was excluded because RGC activity was delayed due to the latency caused by the slow phototransduction process.

Results

RGC responses to single-pulse electrical stimulation

To assess RGC responses to photovoltaic stimulation at various light intensities, we applied isolated 4-ms laser pulses over *n=120* trials to an implant gently pressed onto an RCS retina above

the MEA. In P200 rats, four types of responses could be distinguished by their excitatory and inhibitory phases (Figure 1). Majority of cells (N=41/58) exhibited type 1 response (Figure 1A), and generally they were more abundant near the center of the implant. The most notable feature in this response type is the presence of two inhibitory phases at high irradiances, including a short-latency complete suppression of spontaneous firing, and a delayed long inhibition, which could last for 250 ms. The first inhibitory phase has a lower stimulation threshold than the proceeding peak. A considerable number of cells had similar responses, but did not feature the delayed inhibition. This could be attributed to the separation of the cell from the center of the implant, at which the electrical stimulation did not reach the inhibition threshold.

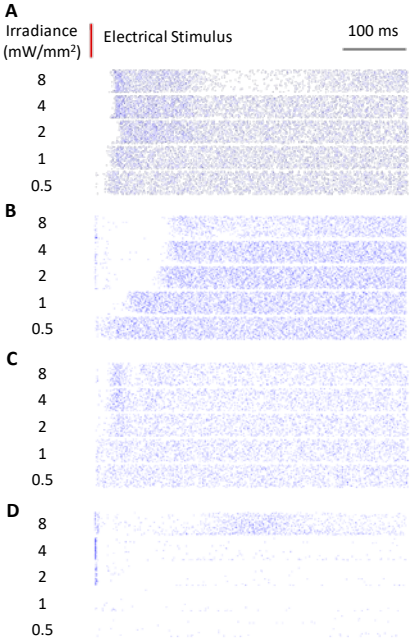

Figure 1. Four types of RGC responses to single pulse stimulation.

The signature of response type 2 (N=6/58, Figure 1B) was its short-latency long-duration inhibition that could extend up to 100 ms post-stimulus. The short latency peak appeared from intermediate irradiances (2 mW/mm^2). Since the data during the first 8.25 ms following the electrical pulse was discarded due to electrical artifact (see Methods), shorter latency responses could not be observed.

Response type 3 (N=5/58, Figure 1C) exhibited initial inhibition, followed by an excitatory peak. At high light intensities, a second period of inhibition and excitation can be observed. Oscillatory activity in the degenerate retina can be due to the amacrine cells[22], and this type of response may be a manifestation of these oscillations. It is not completely clear whether this response is a weak type 1 response superimposed on an oscillatory pattern, or a completely distinct phenomenon.

A very distinct response type could be found in cells with low spontaneous firing rate. This type (N=6/58, Figure 1D) has higher threshold than the other responses. At intermediate intensities, a short low-latency peak appears immediately after the blanking period. As the intensity increased further, long spread-out peak appeared, spanning from 150ms to 380ms. The peak time and duration resembles that of the second inhibition period in type 1 cells.

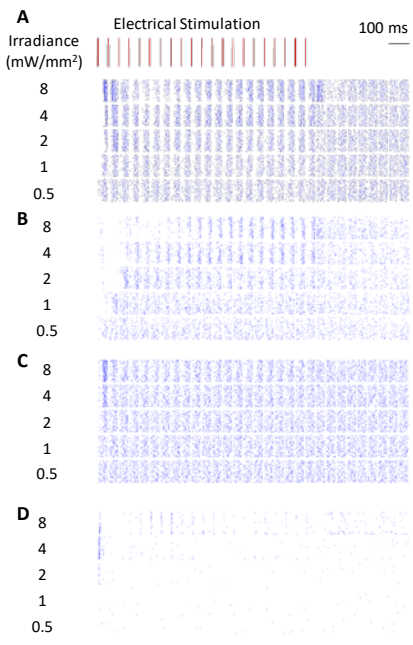

Figure 2. Four types of RGC responses to repetitive stimulation at 20 Hz.

RGC responses to repetitive electrical stimulation

Cells responding to a 1 second burst of 4-ms NIR pulses repeated at 20 Hz were cross-identified using EIs obtained with their single-pulse stimulation, and their responses are shown in Figure 2. Due to artifact removal, 8.25-ms time intervals are excluded in every 50ms long cycle, creating empty vertical strips in the raster plot.

In response type 1, the short latency inhibition occurred after every pulse at all measured irradiances. Excitatory responses appeared at irradiances above 2 mW/mm^2. Delayed transient inhibition occurs at 8 mW/mm^2, and the timing of maximal inhibition aligns with that observed during single-pulse stimulation. The long inhibition in response type 2 was mostly transient under fast repetitive stimulation. Type 3 cells showed strong response only on the first pulse, and very quickly adapted to the repetitive stimulus. Unlike type 1 and 2, the adapted state of these cells includes spiking rate similar to spontaneous firing, with only mild modulation by the periodic stimulus. Typically, this type of cell has higher stimulation thresholds than types 1 and 2. In type 4 cells, the first peak appeared immediately after the first pulse of the stimulus, and only at high irradiance it was repeated after every pulse during about half-a-second.

Contrast Sensitivity

To measure contrast sensitivity of a healthy retina, we projected full-field white light stimuli, varying the irradiance every second. Similar measurements were performed with photovoltaic stimulation of RCS retina, using 1-second-long bursts of 4-ms pulses at 20-Hz with variable intensity. Visual OFF cells responded to lowest levels of contrast (Figure 3). Previously, contrast sensitivity assessment ex-vivo[13] was based on increase in the spiking rate relative to spontaneous firing. To include other aspects of the retinal response, such as inhibitory behavior, we applied a new metric: comparing the spike rate distribution within 25 - 250 ms of a contrast step to spontaneous activity (2-sample K-S test). Low p value indicates the difference in temporal distribution of spiking within the two patterns. Under this metric, visual OFF cells ramp up rapidly from 0 to 3% contrast, and reach plateau above 5% contrast (Figure 3). The full width at half minimum (FWHM) in (1-*p*)-value for visual stimulation corresponded to 2.5% contrast.

Response to electrical stimulation steps had higher threshold and increased over a wider range (Figure 4A). The thresholds agree across different levels of degeneration. An OFF contrast step transitioned a cell from one adapted state to another faster than the ON step. For each contrast step, we compared the spike rate distribution 250 ms before and after the change in irradiance. Stimulation efficacy strongly depends on proximity of the implant to the retina. This effect is

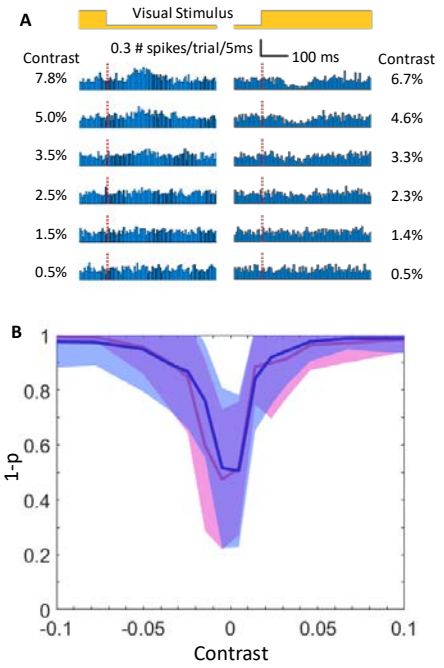

Figure 3A. PSTH of a type-1 cell to ON and OFF visual contrast steps. **B**. Contrast sensitivity. The vertical width of each color band is +/- one sigma for each contrast level.

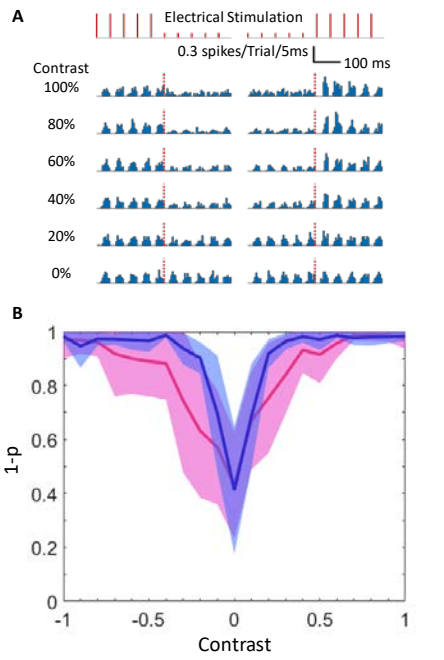

Figure 4A. PSTH of a type-1 cell to ON and OFF electrical contrast steps. **B.** Contrast sensitivity with electrical stimulation.

illustrated by the difference in contrast sensitivity between the two preparations with P200 RCS rats (Figure 4B). Prosthetic responses of degenerate retinas had significantly lower contrast sensitivity than with natural vision: FWHM was 17%, and the (1-*p*) values at +17/-10% contrast in electrical stimulation corresponded to +/-2% contrast in visual stimulation, respectively.

2. Manufacturing of the optimized photovoltaic arrays with pixel sizes down to 40 μm

Introduction

Network-mediated stimulation of the retina with subretinal implants allows preservation of several important features of natural vision, including flicker fusion at high frequencies (>20Hz), adaptation to static images, and non-linear summation of sub-units in receptive fields of RGCs, which enables high spatial resolution[23]. We have demonstrated that with 70μm pixels, prosthetic visual acuity in rats blinded by retinal degeneration matches the pixel pitch [23], and cortical responses are maintained for the life of animals (1-year post implantation).

After development of SiC protective coating to ensure long-term stability of the implant in-vivo[24], this technology is being transferred to Pixium Vision, a company which is preparing it for a clinical trial. Using arrays with 70μm pixels, we hope to achieve spatial resolution corresponding to 20/250 acuity.

Since the acuity matched the pixel pitch and stimulation thresholds were much lower than the ocular safety limits[21, 25], we are developing even smaller pixels, and plan to test the limits of prosthetic vision in animal models of retinal degeneration. Doubling the pixel density would enable spatial resolution corresponding to 20/120 visual acuity. This would make retinal prosthetics applicable not only to relatively few RP patients, but to millions of patients with loss of central vision due to late-stage AMD (geographic atrophy).

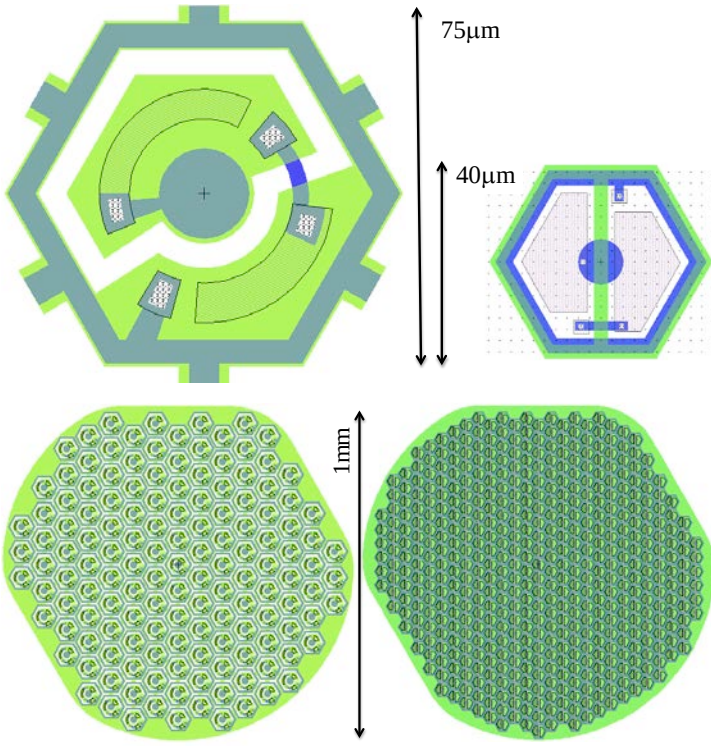

Figure 5. By eliminating the open trenches surrounding the pixels, reducing the width of the isolating trenches from 5 to 1 μm, and decreasing the size of the diodes, we will reduce pixel pitch from 75 to 40 μm. This should enable placement of more than 10,000 pixels within 20° of the visual field.

Methods and Results

The 5μm-wide open trenches between the pixels in our original design were essential for ex-vivo experiments on multi-electrode arrays since they enable diffusion of oxygen and nutrients to the retina sandwiched between the stimulating and recording arrays. However, experiments in-vivo demonstrated that implants without trenches are well tolerated in the animal since the

inner retina is supplied by oxygen and nutrients via the retinal vasculature above the implant. Therefore, we eliminated these trenches and increased pixel density. In addition, each diode in the pixel was isolated by the surrounding 5μm-wide isolation trench (white area in Figure 5A). We now developed technology for producing 1μm-wide trenches filled with SiO_2 in 30 μm-thick silicon, corresponding to aspect ratio of 30:1 (Figure 6). This allows saving a significant fraction of the chip area, and thereby increasing the pixel density. Based on the current stimulation thresholds, and on a computational model of the photovoltaic pixels[26], we project that pixel size can be decreased to 40μm. Therefore, in addition to 70μm pixels, we are producing 55 and 40μm pixels using this technology (Figure 5). It will allow providing more than 10,000 pixels within 20 degrees of the visual field in a human eye, and may enable spatial resolution corresponding to 20/120 visual acuity. If successful, this would make photovoltaic implants applicable not only to RP patients, but also to much larger population of the visually impaired, including millions of people with loss of central vision due to geographic atrophy.

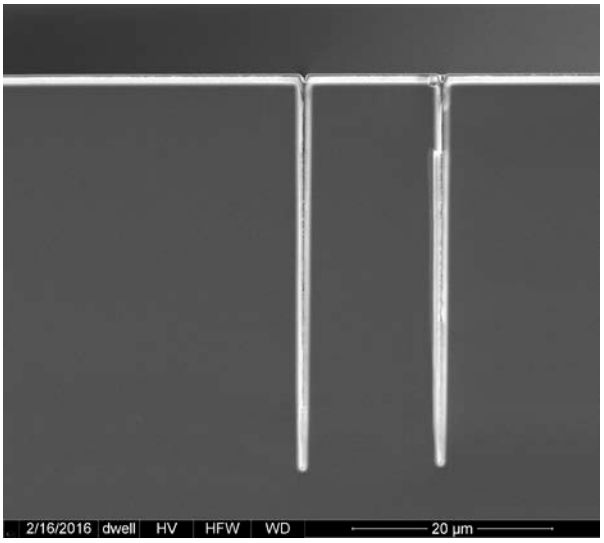

Figure 6: Two trenches of 1μm in width and 45 μm in depth etched in silicon wafer and filled with thermal oxide.

More compact design of the 55μm pixels provides similar photodiode area to the current 70μm pixels. Pixels of 40μm in width (Figure 5) have twice smaller photodiode area, but, since the current stimulation thresholds (0.33 mW/mm^2, 10 ms) are much lower than the safety limits, we can afford doubling the light intensity. More limiting factor in this case becomes the size of the active electrode rather than photodiode area. Currently, with 70μm pixels, the active electrode is 18μm in diameter[23]. With 55 μm pixels, it is decreased to 14μm, and in 40 μm pixels – to 10μm. According to computational modelling of the photovoltaic pixel[26], we should be able to stimulate retinal neurons using 40μm pixels (twice smaller photodiode area and 3.3 times smaller electrode area than in the current 70 μm pixels) while staying below the 5 mW/mm^2 light intensity, planned to be the maximum irradiance in the goggle projection system for human use[25].

In addition to NIR light intensity, two additional factors limit the stimulation thresholds: size of the stimulating electrodes and proximity to the target neurons[30]. We are improving both factors by adding the third dimension to electrodes using electroplated pillar electrodes. We demonstrated retinal migration into 3-D implants several years ago[31], and proposed the concept of pillar electrodes to improve proximity to the inner retinal neurons. Trying to implement them, we explored

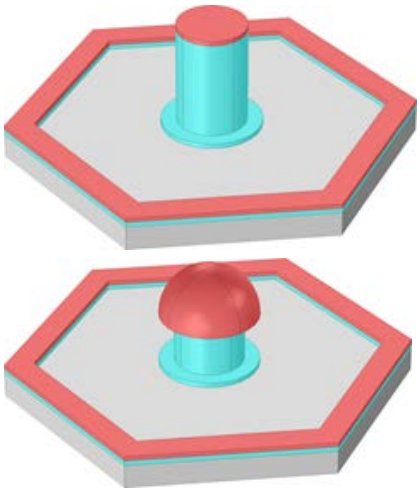

Figure 7. Pillar electrodes with flat top and with a hemispherical dome (bottom). Electrodes are coated with SIROF (red).

multiple fabrication technologies, but integration of the conductive pillars with photodiode arrays was elusive until now. Recently we developed electroplating and 3-D lithography that enabled fabrication of conductive pillars on top of the active electrodes, and SIROF deposition on top of them as well as on the return electrodes at the base of the pixels. Electroplating enables not only control of the pillar height, but also creating the hemispherical top, which doubles the surface area, compared to a flat disk of the same diameter. Example of the electroplated pillar with rounded top is shown in Figure 8.

Figure 8. Electroplated electrodes with 10μm wide pillars and rounded tops.

Electroplating is fully compatible with the rest of the fabrication process, and allows several additional beneficial features. To provide overlap of the sacrificial layer of metal which conducts current to the electrodes during electroplating, we start with pillars of smaller diameter than the active electrodes. With vertical pillars, it results in the top electrode been smaller than the active electrode at the base of the pixel, as shown in Figure 7A. However, we can expand the electrodes by adding a wider cap, as shown in Figure 7B and 8. Hemispherical caps have twice larger surface area than flat disks of the same diameter, thereby increasing the maximum injectable charge from the active electrodes. In addition, hemispherical tops eliminate sharp corners on the flat pillars, which sometimes catch the retina during implantation.

To provide sufficient capacitance, both active and return electrodes in our arrays will be coated with sputtered iridium oxide (SIROF)[22]. This material has proven efficient for retinal stimulation and stable during a year-long follow-up in-vivo [23]. Capacitance of this material is on the order of 1 mF/cm^2 [26] – two orders of magnitude larger than that of polished metal electrodes in electrolyte (10 μF/cm^2), and about an order of magnitude larger than that of Pt grey (~100 μF/cm^2). Due to much larger capacitance of this coating, current will be ejected primarily from the coated top of the pillar, rather than from its flat Pt side walls[35]. This effect eliminates the need for insulation of the side walls, thereby greatly simplifying the fabrication process.

Difficulty with patterned coating of 3-D devices is in the fact that SIROF should be deposited on active and return electrodes located at different heights. This implies that patterns for lift-off of the residual SIROF should be well-defined for both planes (pillar tops and the base). We are solving this problem by utilizing the fact that tops of our pillars are wider than the base, which creates shadowing around the pillar base, thereby helping with the lift-off process.

Dissemination of the Results

Peer-reviewed publications

1. High Resolution Photovoltaic Subretinal Prosthesis for Restoration of Sight. H. Lorach and D. Palanker. Chapter 9 in "Artificial Vision: a Clinical Guide". P. Gabel (Editor).
2. Electronic Approaches to Restoration of Sight. G. Goetz and D. Palanker. Reports on Progress in Physics 79: 096701 (29pp) (2016)
3. SiC protective Coating for Photovoltaic Retinal Prosthesis. X. Lei, S. Kane, S. Cogan, H. Lorach, L. Galambos, P. Huie, K. Mathieson, T. Kamins, J. Harris and D. Palanker. Journal of Neural Engineering 13: 046016 (12pp) (2016).

4. Optimization of Return Electrodes in Neurostimulating Arrays. T. Flores, G. Goetz, X. Lei, and D. Palanker. Journal of Neural Engineering 13: 036010 (11pp) (2016).
5. Implantation of Modular Photovoltaic Subretinal Prosthesis. D.Y. Lee, H. Lorach, P. Huie, D. Palanker. Ophthalmic Surgery, Lasers and Imaging Retina. 47: 171-174 (2016).
6. Photovoltaic Pixels for Neural Stimulation: Circuit Models and Performance. D. Boinagrov, X. Lei, G. Goetz, T.I. Kamins, K. Mathieson, L. Galambos, J.S. Harris, and D. Palanker. IEEE Trans. Biomed. Circuits and Systems 10(1): 85-97 (2016).

Conference presentations

1. Photovoltaic restoration of sight in rodents with retinal degeneration. Daniel Palanker; SPIE, Photonics West, San Francisco, 2017
2. Photovoltaic restoration of sight in rodents with retinal degeneration. Henri Lorach, Dae-Yeoung Lee, Xin Lei, Roopa Dalal, Theodore Kamins, Ludwig Galambos, James Harris, Daniel Palanker; The Eye and The Chip. Biannual International Symposium on Artificial Vision. Detroit, 2017.
3. Photovoltaic Restoration of Sight: from Bench to Bedside. D. Palanker, H. Lorach, X. Lei, T. Kamins, J. Harris, K. Mathieson. The Eye and The Chip. Biannual International Symposium on Artificial Vision. Detroit, 2017.
4. Implications of low prosthetic contrast sensitivity for delivery of visual information. Georges Goetz, Richard Smith, Xin Lei, Ludwig Galambos, Theodore Kamins, Keith Mathieson, Alexander Sher, Daniel Palanker; ARVO 2016
5. Robert and Gerry Ligon Lectureship at Vision Research Center, Kresge Eye Institute, Detroit. May 2016 “Photovoltaic Restoration of Sight in Rodents with Retinal Degeneration”
6. Annual Meeting of the Israeli Society for Vision and Eye Research. Ramat Gan, March 2016; “Photovoltaic restoration of sight in animals with retinal degeneration”.

Impact: Shear forces inflicted by explosion or head impact may result in traumatic retinopathy due to damage of the retinal pigmented epithelium and photoreceptors, leading to irreversible loss of sight. In these conditions the inner retinal neurons that process the visual signals and relay them to the brain are relatively well preserved. Patterned electrical stimulation of these neurons can elicit pattern perception, thereby restoring sight. Photovoltaic retinal prosthesis offers a very promising approach to restoration of sight due to its high resolution, wireless nature of the implants, small size, modularity and ease of implantation.

We continue advancing this technology according to the SOW, and transfer technology for commercialization and upcoming clinical trials by Pixium Vision. If successful, we expect the current implants to provide visual acuity on the level of 20/250. We are developing smaller pixels, which might enable visual acuity on the level of 20/120.

Participants & other Collaborating Organizations

Organization Name: Stanford University

**Location of Organization: Hansen Experimental Physics Laboratory,
452 Lomita Mall, Astrophysics Building,
Room S05 & S04, Stanford, CA 94305-4085**

1. Prof. Daniel Palanker

Name:	Daniel Palanker
Project Role:	PI
Nearest person month worked:	2.4 CM
Contribution to Project:	Directs the project, evaluates the results, writes the reports and publications.

2. Mr. Yi Quan

Name:	Yi Quan
Project Role:	Research Associate
Nearest person month worked:	2.4 CM
Contribution to Project:	Helps with animal protocols, tissue processing and immunohistochemistry.

3. Mr. Ludwig Galambos

Name:	Ludwig Galambos
Project Role:	Research Associate/Engineer
Nearest person month worked:	4.5 CM
Contribution to Project:	Works on fabrication of the photovoltaic arrays

4. Ms. Roopa Dalal

Name:	Roopa Dalal
Project Role:	Research Associate (Histologist)
Nearest person month worked:	1.0 CM
Contribution to Project:	Works on tissue fixation, embedding, histological sectioning, staining and microphotography.

5. Ms. Xin Lei

Name:	Xin Lei
Project Role:	Graduate Student
Nearest person month worked:	3.0 CM
Contribution to Project:	Works on design and fabrication of the photovoltaic arrays.

6. Mr. Thomas Flores

Name:	Tom Flores
Project Role:	Graduate Student
Nearest person month worked:	1.5 CM
Contribution to Project:	Works on design and fabrication of the photovoltaic arrays.